BUTTERWORTH HEINEMANN

Polymer Vol. 36 No. 2, pp. 345–351, 1995

0032-3861/95/$10.00 + 0.00

Simulation of non-linear models for polymer chains in flowing solutions

J. J. López Cascales, F. G. Díaz and J. García de la Torre*
Departamento de Química Física, Facultad de Química, Universidad de Murcia, 30071 Murcia, Spain
(Received 21 January 1994; revised 20 May 1994)

Two non-linear bead and spring models are considered for the Brownian dynamics simulation of the behaviour of polymer chains in a dilute solution under shear or elongational flow. One of them is the HYBRID model whose springs are Hookean at low elongation, and beyond some spring length they follow a Morse potential with a given dissociation energy. This model is suitable for studying polymer fracture in strong flows. In this paper we describe the model and check that it has the proper behaviour in the two regions. The second model is a chain of finitely extensible, non-linear elastic (FENE) springs. Our simulations show several features of the FENE model that agree well with observation. In shear flow, the deformation of the FENE chain at high shear rate deviates from the square law followed at low shear, in agreement with some experiments. The model also predicts the typical shear-thinning, non-Newtonian behaviour of the shear viscosity. In elongational flows, the variation of the chain properties with the elongation rate shows a rather sharp increase at some critical rate that is reminiscent of the so-called coil–stretch transition.

(Keywords: Brownian dynamics simulation; dilute solution; bead and spring models)

INTRODUCTION

The behaviour of flexible macromolecular chains in a flowing solution is a difficult subject because of the complex interplay between conformational and hydrodynamic aspects. If one wishes to obtain analytical results, approximations of some kind usually have to be included in the theoretical treatments[1]. Since the early 1980s, the Brownian dynamics simulation technique has proven to be a powerful alternative tool for the study of the behaviour of polymer chains in a solution subjected to any type of flow[2–15]. In particular, we have studied the deformation, orientation, birefringence and viscosity of polymer chains in shear flows[9–13] as well as the interesting processes of sudden polymer stretching and fracture in elongational flow[14,15]. The polymer model used in our previous studies has mainly been the simple Rouse bead and spring model with Hookean springs, Gaussian statistics and infinite extensibility. This model is commonly accepted as a proper representation of polymer chains at low flow rates, and in Brownian dynamics simulation it has the advantage of allowing quite large time steps Δt owing to the linear and 'soft' nature of the springs. When we were concerned with deformation and fracture in strong elongational flows, we employed another model with springs obeying a Morse potential[14,15] that includes dissociation behaviour. At low energy, the Morse chain reduces to a chain of 'hard' Fraenkel[1,16] springs with non-zero equilibrium length and a large spring constant. This requires the use of a small Δt in the simulation, with a corresponding increase in computing time.

In the present paper we consider two alternative chain models in the Brownian dynamics (BD) simulations. One of them is the HYBRID model which combines the desirable features of the Hookean (Gaussian) springs at low elongation with dissociation behaviour at high energies, thus enabling the use of fairly large time steps in both regimes. In addition to the HYBRID model, which is original in the present work, we have also considered the well-known finitely extensible, non-linear elastic (FENE) model[1,17], which had not been used in BD simulations until very recently[8]. Essentially, we carry out for both models a series of simulations similar to those that we have previously made with Gaussian and Morse models. We check whether the HYBRID model actually describes properly the two regimes, and from the results from the FENE model with a non-approximate inclusion of hydrodynamic interaction (HI) we learn about the joint influence of finite extensibility and HI on the deformation of the polymer chain and the non-Newtonian behaviour of the polymer solution.

MODELS AND SIMULATIONS

The system under study is a very dilute solution of high molecular weight polymers which is subjected to some type of flow. We model the polymer as a chain with N beads of radius σ (which represents the friction of the polymer with the solvent) connected by $N-1$ springs describing the internal degrees of freedom. Two different types of springs, HYBRID and FENE, are considered.

HYBRID model

We propose in this work a HYBRID model in which the springs show linear or elastic (Hookean) behaviour for low elongations until the spring length Q reaches a

* To whom correspondence should be addressed

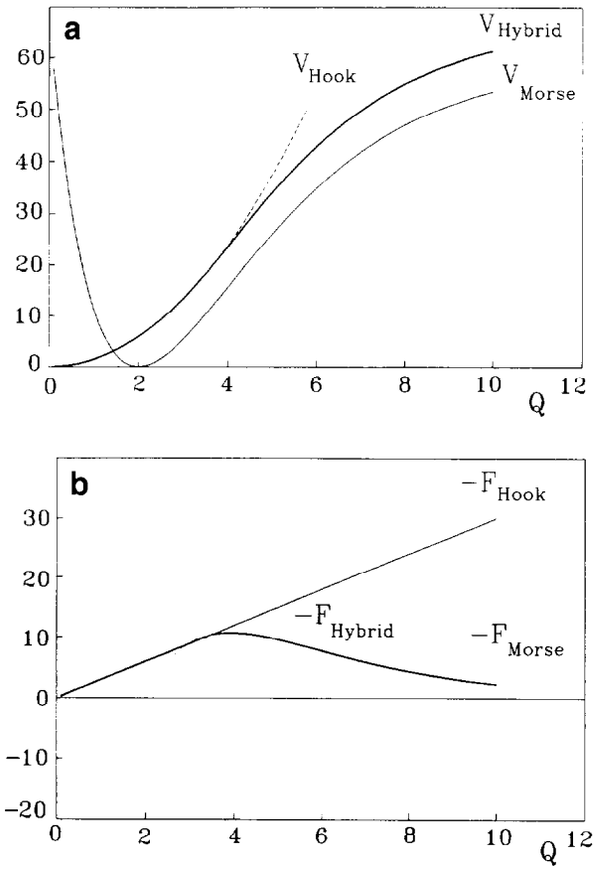

Figure 1 Potentials (a) and forces (b) for Gaussian, Morse and HYBRID models (curves corresponding to $H=3$, $A=60$ and $b_0=2$ in reduced units)

certain value Q_c, and beyond this value inelastic forces of the Morse type are applied. Thus, the potential energy and the force at the HYBRID springs are given by

$$V(Q)=\begin{cases} HQ^2/2 & Q\leqslant Q_c \\ A[1-e^{-B(Q-b_0)}]^2+\Delta V(Q_c) & Q>Q_c \end{cases} \quad (1a)$$

and

$$F(Q)=\begin{cases} -HQ & Q\leqslant Q_c \\ 2AB[e^{-2B(Q-b_0)}-e^{B(Q-b_0)}] & Q>Q_c \end{cases} \quad (1b)$$

The Hookean constant is $H=3kT/\langle Q^2\rangle_G$, where $\langle Q^2\rangle_G$ is the mean-square spring length in the case that $F(Q)$ is Hookean for all spring lengths. (Actually, the contribution of the Morse part to $\langle Q^2\rangle$ is negligible because it takes place at high energies that are statistically insignificant, and therefore we can accept that $H=3kT/\langle Q^2\rangle$ directly.) A is the dissociation energy of the springs: note that $V(Q)-\Delta V(Q_C)\rightarrow A$ as $Q\rightarrow\infty$. The two other Morse parameters lose the meaning that they have in a pure Morse potential since they determine the behaviour at low Q, when the potential is not represented by Morse equations. In any case, numerical values have to be assigned to them. Regarding the crossover from the Hookean region to the Morse region, we stipulate that $V(Q)$ and its first derivative $F(Q)$ must be continuous. Thus, given numerical values (in dimensionless forms; see below) for H on the one hand and A and b_0 on the other, B and Q_C are fixed by the continuity of $F(Q)$ (the Hooke and Morse equations for $F(Q)$ must have a single contact point instead of none or two). Values for B and Q can be found by an iterative procedure. The continuity in $V(Q)$ requires a shift upwards of the Morse part, adding $\Delta V(Q_c)$, which is just the difference between the pure Hookean and Morse potentials at Q_c, i.e.

$$\Delta V(Q_c)=(HQ_c/2)-A[1-e^{-B(Q_c-b_0)}]^2 \quad (2)$$

Figure 1 illustrates how the HYBRID model is constructed from the Hookean and Gaussian curves for $F(Q)$ and $V(Q)$.

FENE model

For the finitely extensible, non-linear elastic (FENE) spring model[1,17], the potential energy and force are given by the well-known expressions

$$V(Q)=-HQ_0^2\ln[1-(Q/Q_0)^2]/2 \quad (3a)$$

and

$$F(Q)=-HQ/[1-(Q/Q_0)^2] \quad (3b)$$

where H is the spring constant, as in the previous model, and Q_0 is the maximum length of the springs. There are a number of approximate versions of the FENE model in the literature, such as the FENE-P and FENE-PM models[18] which are based on the so-called Peterlin approximation. These versions were proposed to simplify the analytical development and the numerical handling. However, there is no need to employ such approximations in Brownian dynamics simulation, and therefore we employ here the original FENE model.

Brownian dynamics

We employ the computer simulation technique known as Brownian dynamics, and particularly the Ermak–McCammon[19] algorithm improved by Iniesta and García de la Torre[20] with a second-order modification. In our simulations, each step is calculated according to

$$\mathbf{r}_i=\mathbf{r}_i^0+(\Delta t/kT)\sum_j \mathbf{D}_{ij}\cdot\mathbf{F}_j+\mathbf{V}_i^0\cdot\Delta t+\boldsymbol{\rho}_i(\Delta t) \qquad i=1,\ldots,N \quad (4)$$

where $\mathbf{r}_i^0$ is the position vector for bead i before the Brownian step, Δt is the time period, kT is the Boltzmann factor, $\mathbf{D}_{ij}$ is the diffusion tensor (given by the Rotne–Prager–Yamakawa[21,22] expression in our case), $\mathbf{F}_i$ represents the forces on bead i, $\mathbf{V}_i$ is the velocity of the solvent at the position of this sphere and $\boldsymbol{\rho}_i$ is the random contribution to the Brownian motion.

The flow is introduced into the algorithm through the term $\mathbf{V}_i$, and its value depends on whether we simulate shear or elongational flow. For shear flow

$$V_x=y\dot{\gamma},\ V_y=V_z=0 \quad (5a)$$

and for elongational flow

$$V_x=-\dot{\varepsilon}x/2,\ V_y=-\dot{\varepsilon}y/2,\ V_z=\dot{\varepsilon}z \quad (5b)$$

where $\dot{\gamma}$ and $\dot{\varepsilon}$ are shear and elongation rates.

In simulation it is convenient to work with dimensionless magnitudes instead of the real values. This is accomplished by dividing the basic quantities by the length l, which is the root-mean-square length of the springs in the Gaussian limit, the energy kT and the time $l^2\zeta/k_BT$. In these units the parameters used in the simulation are $H^*=3$ and $\lambda_H^*=0.083$, where λ_H is a

characteristic time given by $\lambda_H = \zeta/4H$ and normalized according to inverse time units. For one of the Morse parameters we take, as in our previous work, $A^* = 60$. With a reasonable choice of $b_0^* = 2$, the two other Morse parameters are determined to be $B^* = 0.35$ and $Q_C^* = 3.5$. For the FENE model we take $Q_0^* = 10$, and therefore the b parameter in the FENE springs ($b = HQ_0^2/k_BT$) takes the dimensionless value $b^* = 300$. The hydrodynamic radius of the beads $\sigma^* = 0.257$, which corresponds to a value of the HI parameter h^* of 0.25, where $h^* = (3/\pi)^{1/2}\zeta/6\pi\eta_0 b$.

For the simulation conditions we use 10^6 steps divided into five subtrajectories (2×10^5 steps each), the first of which is rejected to allow the model to reach the steady state in the presence of the flow[7], and the properties are averaged in the other four subtrajectories, sampling one out of every four steps. A critical parameter in the simulations is Δt^* (mainly in the FENE model) because for high gradients, in which the springs are very stretched, we find important variations in the values of the forces within a single step, and one of the conditions in our technique is that the forces must be constant during a time step. The optimized value for Δt^* is 0.02 for both models at low intensities of flow, and $\Delta t^* = 0.002$ for the HYBRID and FENE models when the intensity is higher.

RESULTS

Steady shear flow

In this type of flow it is convenient to use a form of the shear rate related to the length of the polymer chain[1]

$$\beta = M\eta_s[\eta]_0\dot{\gamma}/N_A k_B T \tag{6}$$

where M is the molecular weight, η_s is the viscosity of the solvent, $[\eta]_0$ is the intrinsic viscosity of the solution when no flow is present and $\dot{\gamma}$ is the shear rate. Using dimensionless parameters we can write

$$\beta = [\eta]_0^*\dot{\gamma}^*/6\pi\sigma^* \tag{7}$$

where

$$\dot{\gamma}^* = (6\pi\eta_s\sigma l^2/kT)\dot{\gamma} \tag{8}$$

and $[\eta]_0^* = [\eta]_0 M/N_A l^3$ is the reduced intrinsic viscosity.

We start our study with the influence of the shear rate β on the relative increase ϕ in the mean-square radius of gyration, defined as

$$\phi = \left(\frac{\langle S^2\rangle}{\langle S^2\rangle_0}\right) - 1 \tag{9}$$

where $\langle S^2\rangle$ is the radius of gyration for a shear rate β and $\langle S^2\rangle_0$ is the value for zero shear rate.

In *Figure 2* for the FENE model we show log–log plots of ϕ *versus* β with (HI) and without (no HI) hydrodynamic interaction. The aspects of these plots are different from those obtained when the Gaussian model is used[12]. At low shear rate, the deformation ϕ in both cases follows a straight line in the log–log plot with a slope close to 2, indicating that the known power law

$$\phi = C\beta^2 \tag{10}$$

for Gaussian chains holds for the FENE chains at low β. Indeed, the numerical values that we find for the constant, $C_{noHI} = 0.15$ and $C_{HI} = 0.09$, are practically the same as those found for the Gaussian chain[12,23]. This indicates that in the low shear region the ϕ–β relationship is model independent.

However, at high shear rate a downward curvature appears in the plots, so that equation (10) is not valid in this region. It is important to point out that this behaviour matches precisely that observed experimentally by Lindner and Oberthür[24] using low angle neutron scattering for polystyrene in shear flow, with a clear deviation from equation (10) at high shear. The origin of the deviation, about which there has been some hypothesis, can therefore be explained (among other factors) in terms of the finite extensibility of the polymer chain.

We have also calculated the intrinsic viscosity for the FENE model. The contribution of the polymer to the solution viscosity is

$$\eta - \eta_s = -(\tau_{xy})_p/\dot{\gamma} \tag{11}$$

where $(\tau_{xy})_p$ is the contribution of the polymer to the xy component of the stress tensor. Then, the intrinsic viscosity $[\eta]$ is given by

$$[\eta] = \lim_{c\to 0}\left(\frac{\eta - \eta_s}{c\eta_s}\right) = -\frac{N_A}{\eta_s nM}\frac{(\tau_{xy})_p}{\dot{\gamma}} \tag{12}$$

where n and c are, respectively, the number concentration and mass concentration of the polymer. Using the modified Kramers[1,25] stress tensor for a macromolecular model based on beads and springs, the intrinsic viscosity

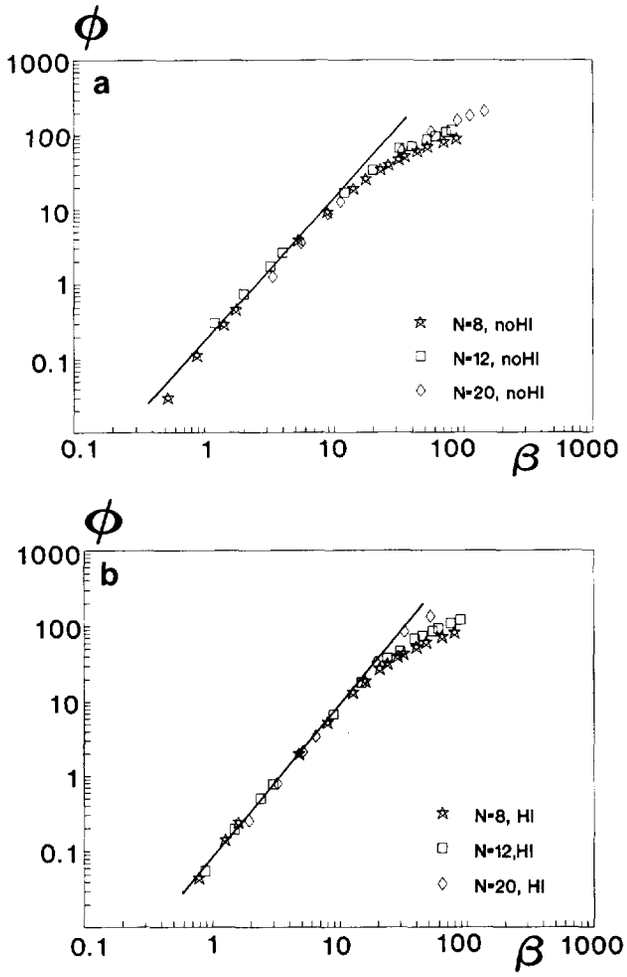

Figure 2 Variation of the conformational parameter ϕ for the FENE model in shear flow *versus* the shear rate β without (a) and with (b) hydrodynamic interaction

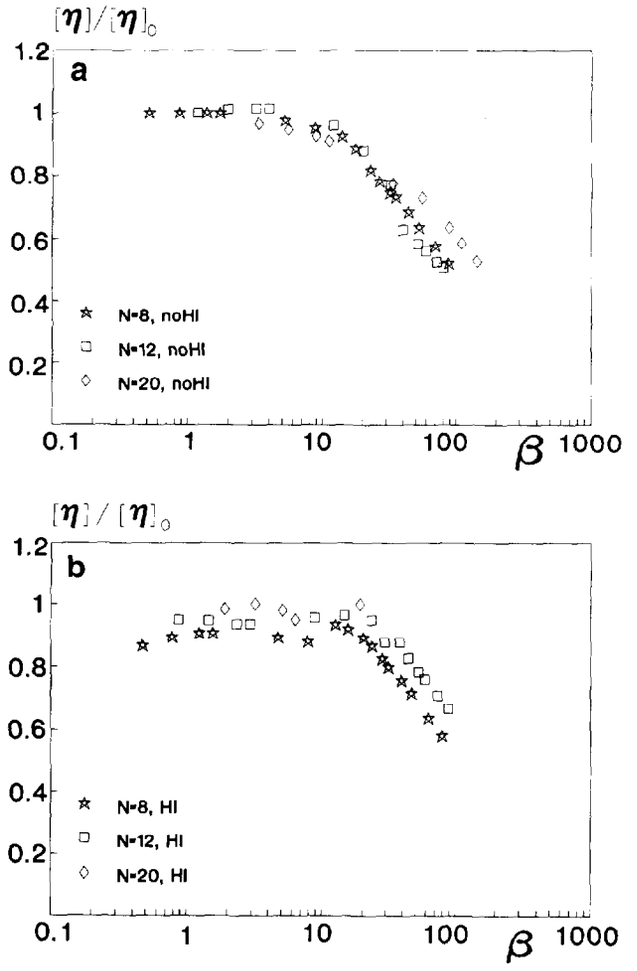

Figure 3 Variation with shear rate β of the shear viscosity $[\eta]$ normalized to its value at zero shear rate $[\eta]_0$ for the FENE model without (a) and with (b) hydrodynamic interaction

can be calculated by means of

$$[\eta] = \frac{N_A}{\eta_s n M \dot{\gamma}} \sum_{i=1}^{N} \langle R_{i,x} F_{i,y}^{(m)} \rangle \tag{13a}$$

or

$$[\eta]^* = (6\pi\sigma^*/\dot{\gamma}^*) \sum_{i=1}^{N} \langle R_{i,x}^* F_{i,y}^{(m)*} \rangle \tag{13b}$$

where N_A is the Avogadro constant, M is the molecular weight of the polymer, R_i is the position vector of bead i relative to the centre of mass of the chain and $F_i^{(m)}$ denotes the 'mechanical' forces which act on bead i, obtained as the composition of the forces associated with the springs connected to that bead.

In *Figure 3* we show the variation of the intrinsic viscosity $[\eta]$ for different chain lengths ($N = 8$, 12 and 20), normalized to the value in the absence of flow $[\eta]_0$, *versus* the intensity of the flow (in terms of β) for the no HI and HI cases. In both cases we note the typical non-Newtonian behaviour with shear thinning at high values of β. This is in contrast to the Newtonian behaviour of the Gaussian model without HI, and with the non-Newtonian positive deviation (shear thickening) with HI[11,26]. Therefore, finite extensibility seems to be a factor of more importance than the inclusion of the hydrodynamic interaction in the prediction of the non-Newtonian behaviour of polymer solutions.

In the HYBRID model the variations in $\langle S^2 \rangle$ and $[\eta]$ are very similar to those shown by the Gaussian model with and without HI, as we can see in *Table 1* for the particular case of $N = 12$ and different shear rates. The only difference to be pointed out is that it is not possible to apply high gradients of flow to our model because this could produce fracture of the chain. This is the reason why we have not done a particular study for the HYBRID model at high shear rates, and we can assume that all the conclusions (in the range before fracture) are the same as those obtained for the Gaussian model[10,12,26].

Steady elongational flow

Steady elongational flow is the second type of flow we studied in the present work. First, we show some results for $\langle S^2 \rangle$ and the elongational viscosity $[\bar{\eta}]$ for the FENE and HYBRID models in steady state, followed by a brief presentation of the kinetics of fracture for the HYBRID model.

The elongation rate $\dot{\varepsilon}$ can be recast in a dimensionless form ν in the same way as done for β in equation (6)

$$\nu = M\eta_s[\eta]_0\dot{\varepsilon}/N_A k_B T \tag{14}$$

where all the parameters have their usual meanings. Using dimensionless parameters we have

$$\nu = \frac{[\eta]_0^*}{6\pi\sigma^*}\dot{\varepsilon}^* \tag{15}$$

where $\dot{\varepsilon}^*$ is defined in terms of $\dot{\varepsilon}$ as in equation (8).

In *Figure 4* we show the elongation rate dependence of $\langle S^2 \rangle$ expressed in terms of the deformation ϕ for the FENE model with different chain lengths ($N = 8$, 12 and 20) with and without HI. From these data we observe a first range of ν in which there is nearly no change in the coil conformation of the polymer chain with elongation rate up to a certain value ν_c, where a sudden change in coil conformation is produced and the chain adopts a much more stretched state. This behaviour is sometimes regarded as a coil–stretch transition, although such a transition can also be considered as a kinetic process in the sense that it is a temporal change from one conformation to the other, which requires some minimum intensity of flow ν_c. To quantify a possible scale law for the relationship between ν_c and the chain length N (or molecular weight) from our results, we first note (according to *Figure 4*) that the value of ν_c is independent of N, both with and without hydrodynamic interaction. (Actually, we observe $\nu_c \approx 1$ both with and without HI.) Now,

Table 1 Values of the mean-square radius of gyration $\langle S^2 \rangle$ and shear viscosity $[\eta]$ for Gaussian and HYBRID models (both in dimensionless form) corresponding to a chain length of $N = 12$ with and without HI

	No HI				HI			
	HYBRID		Gaussian		HYBRID		Gaussian	
$\dot{\gamma}^*$	$\langle S^2 \rangle^*$	$[\eta]^*$	$\langle S^2 \rangle^*$	$[\eta]^*$	$\langle S^2 \rangle^*$	$[\eta]^*$	$\langle S^2 \rangle^*$	$[\eta]^*$
0.3	2.51	19.01	2.53	19.4	2.21	14.2	2.15	13.8
0.5	2.51	19.1	3.37	19.5	2.51	13.9	2.47	13.4
0.8	5.3	19.1	5.4	19.6	3.3	13.6	3.10	13.1
1.0	–	–	–	–	3.8	13.6	3.62	13.4

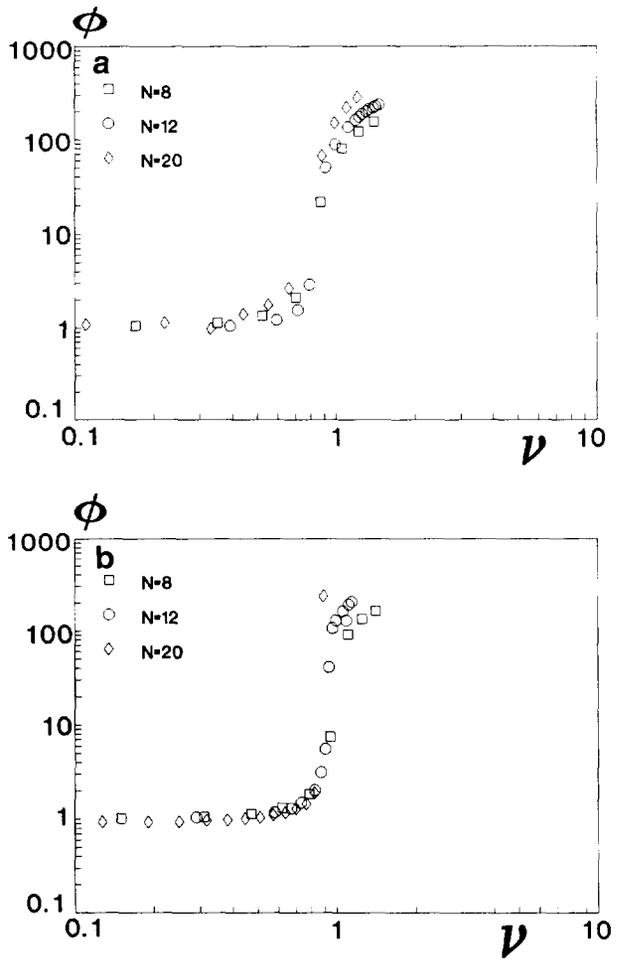

Figure 4 Variation of the conformational parameter ϕ for the FENE model in elongational flow *versus* the elongation rate ν with (a) and without (b) hydrodynamic interaction

according to equation (15), ν is proportional to the intrinsic viscosity in the absence of flow

$$\nu \propto [\eta]_0^* \dot{\varepsilon}^* \tag{16}$$

and taking into account that $[\eta]_0^*$ varies differently with the chain length depending on our consideration of HI[14], i.e.

$$[\eta]_{0,\text{noHI}}^* \propto N^2 \tag{17a}$$

and

$$[\eta]_{0,\text{HI}}^* \propto N^{3/2} \tag{17b}$$

we obtain, combining equations (16) and (17) and making use of the observation that ν_c is independent of chain length

$$(\dot{\varepsilon}_c)_{\text{noHI}} \propto N^{-2} \tag{18a}$$

and

$$(\dot{\varepsilon}_c)_{\text{HI}} \propto N^{-3/2} \tag{18b}$$

Experimentally[27,28] it is obtained that $\dot{\varepsilon}_c \propto N^{-3/2}$, which is in perfect agreement with our simulation results in the presence of hydrodynamic interaction. We recall that for a chain of Morse springs there is a dissociation (or fracture) limit, but the rise in chain dimensions is not as sharp as in FENE chains, and therefore we did not discuss ν_c for Morse chains in our previous work[14]. On the other hand, the need to introduce HI into the model to reproduce the experimental result is evident.

Studying the hydrodynamic behaviour, we will pay attention to the elongational viscosity $\bar{\eta}$. This property can be calculated from[1]

$$\bar{\eta} = (\tau_{xx} - \tau_{zz})/\dot{\varepsilon} \tag{19}$$

where τ_{xx} and τ_{zz} are the normal components of the stress tensor of the solution. As in the case of shear flow, we are interested in the contribution of the polymer to the viscosity of the solution as measured by the elongational intrinsic viscosity $[\bar{\eta}]$. Using again the Kramers[25] tensor we obtain

$$[\bar{\eta}] = \frac{N_A}{\eta_s M \dot{\varepsilon}} \sum_{i=1}^{N} \langle R_{i,x} F_{i,x}^{(m)} - R_{i,z} F_{i,z}^{(m)} \rangle \tag{20}$$

and

$$[\bar{\eta}]^* = (6\pi\sigma^*/\dot{\varepsilon}^*) \sum_{i=1}^{N} \langle R_{i,x}^* F_{i,x}^{(m)*} - R_{i,z}^* F_{i,z}^{(m)*} \rangle \qquad i = 1, \ldots, N \tag{21}$$

where $R_{i,\alpha}$ and $F_{i,\alpha}^{(m)}$ ($\alpha = x, y$ or z) and their dimensionless forms have the same meanings as in equations (13).

From our simulations for the FENE model we have obtained the variations in $[\bar{\eta}]$ *versus* ν with and without HI. In both cases we can observe an important change in the viscosity for a certain value of ν that coincides with ν_c for the coil–stretch transition of the chain as shown in *Figure 5*, where we have considered only the HI case. At very high $\dot{\varepsilon}$, the properties of the FENE model are expected to reach a plateau or limit corresponding to a nearly linear chain with spring lengths close to Q_0. This is indeed predicted by other calculations[18,29]. In our simulations we cannot approach that limit because these forces are very strong and the algorithm becomes unstable (a much smaller Δt would be required). Anyhow, our results in *Figures 4* and *5* show, after the sudden increase, an inflection that suggests the expected trend.

For the HYBRID model with $N = 20$, we show in *Table 2* the values of $\langle S^2 \rangle^*$ and $[\bar{\eta}]^*$ for different intensities of flow. They show variations similar to those shown by the Gaussian model. However, the existence of a certain value $\dot{\varepsilon}_f$ above which the polymer chain

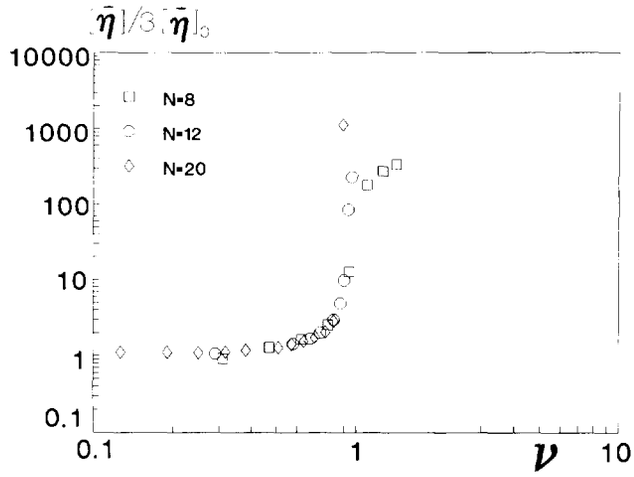

Figure 5 Variation with elongation rate ν of the elongational intrinsic viscosity $[\bar{\eta}]$ for the FENE model normalized to its value at zero elongation rate $[\bar{\eta}]_0$ and including hydrodynamic interaction

Table 2 Values of the mean-square radius of gyration $\langle S^2 \rangle$ and elongational intrinsic viscosity $[\bar{\eta}]$ for the Gaussian and HYBRID models (both in dimensionless form) corresponding to a chain length of $N = 20$ with and without HI

	No HI					HI			
	HYBRID		Gaussian			HYBRID		Gaussian	
$\dot{\varepsilon}^*$	$\langle S^2 \rangle^*$	$[\bar{\eta}]^*$	$\langle S^2 \rangle^*$	$[\bar{\eta}]^*$	$\dot{\varepsilon}^*$	$\langle S^2 \rangle^*$	$[\bar{\eta}]^*$	$\langle S^2 \rangle^*$	$[\bar{\eta}]^*$
0.01	3.37	170	3.35	198	0.01	3.21	123	3.17	93
0.03	3.65	228	3.55	255	0.03	3.26	106	3.24	99
0.05	4.66	325	4.4	381	0.05	3.39	115	3.74	131
0.06	5.6	379	4.7	452	0.08	3.76	133	4.0	141
0.07	13.0	1100	14.5	1201	0.1	4.5	172	8.9	207

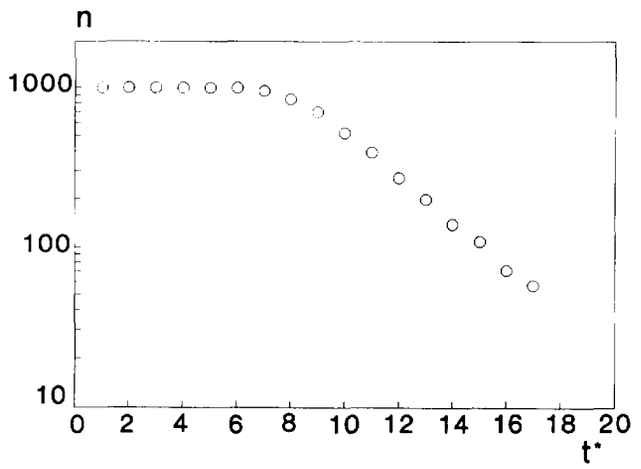

Figure 6 Fracture kinetics of 1000 chains with $N = 20$ for the HYBRID model without hydrodynamic interaction at $\dot{\varepsilon}^* = 0.4$

fractures introduces a substantial difference with respect to the Gaussian model. The difference appears because we have changed the completely elastic behaviour to elastic behaviour with a limit above which the connector cannot be stretched any more and breaks. As a consequence, for $\dot{\varepsilon} > \dot{\varepsilon}_f$ certain connectors can reach Q_c and then follow non-linear behaviour before fracture. Therefore, in this model (different from the Gaussian model[15]) there is a transition from linear to non-linear elasticity and finally to fracture. This simulated process is similar to the real process.

We have done a brief study of the kinetic parameters of fracture for the HYBRID model. We start with the dependence of $\dot{\varepsilon}_f$ on the chain length N. From our results we obtain a clear linear variation when we plot (in a log–log diagram) $\dot{\varepsilon}_f$ *versus* N, and we can express this result as

$$(\dot{\varepsilon}_f)_{noHI} \propto N^{-1.98} \tag{22a}$$

and

$$(\dot{\varepsilon}_f)_{HI} \propto N^{-3/2} \tag{22b}$$

in perfect agreement[14] with the results obtained with both Morse and Gaussian models in the two HI cases. The HYBRID model, therefore, also behaves properly in the prediction of this power law.

Finally, we consider the kinetics of fracture by plotting the number of intact chains n *versus* time for a determined value of $\dot{\varepsilon}^*$ ($\dot{\varepsilon}^* > \dot{\varepsilon}_f^*$). In *Figure 6* we see that this characteristic can be fitted, after a brief induction period, to a first-order law in the form $\ln n = -k_f t + A$, and from the slope of the decay we can obtain the rate constant of fracture k_f. In *Table 3* we show the simulation results for the HYBRID model compared with those from the Morse and Gaussian models[15]. A qualitative comparison can be made by neglecting hydrodynamic interaction, saving a very large amount of computing time. Another interesting study is the determination of the dependence of k_f and the fracture half-time $t_{1/2}$ on $\dot{\varepsilon}_f$. For the HYBRID model we obtain $k_f^* \propto \dot{\varepsilon}^*$ and $t_{1/2}^* \propto (\dot{\varepsilon}^*)^{-1.2}$, in perfect agreement with the findings from the other models. Numerically the value of k_f^* for the HYBRID model is very similar to the Gaussian value, while for $t_{1/2}^*$ the value practically coincides with that from the Morse model. In other words, the HYBRID model shows fracture behaviour that is really hybrid between Gaussian and Morse.

Table 3 Values of the fracture rate constant k_f and fracture half-time $t_{1/2}$ for Gaussian (G), Morse (M) and HYBRID (H) models (in dimensionless form) corresponding to a chain length of $N = 20$ without HI

$\dot{\varepsilon}^*$	$(k_f^*)_H$	$(k_f^*)_G$	$(k_f^*)_M$	$(t_{1/2}^*)_H$	$(t_{1/2}^*)_G$	$(t_{1/2}^*)_M$
0.2	0.13	0.13	–	24.35	33.7	–
0.4	0.37	0.28	0.27	10.15	14.3	10.5
0.5	0.5	0.47	–	7.80	10.0	–
0.6	0.71	0.68	0.42	6.29	8.2	6.4
0.7	0.76	0.88	–	5.26	6.9	–
0.8	0.97	1.11	0.67	4.49	5.8	4.4

CONCLUSIONS

In the present work, we have proved that the finite extensibility of the springs in bead and spring models is important for describing qualitatively different properties of polymer solutions in the presence of flows, as shown by comparison of the FENE and Gaussian models. In particular, for FENE chains the deformation in shear resembles the experimental behaviour, the viscosity shows a typical shear-thinning effect, and in elongational flows there is a sharp variation of properties with elongation rate. Taking into account HI introduces quantitative corrections that approximate our results to the experimental values.

On the other hand, the HYBRID model shows for the whole range of intensities of flow previous to fracture a behaviour similar to that shown by the Gaussian model in the presence of steady flow, but introduces a new improvement for the study of fracture processes that will allow the use of longer Δt values with a consequent decrease in computing time. This will make it possible to run longer simulation experiments, which is presently a serious limitation.

REFERENCES

1 Bird, R. B., Curtiss, C. F., Amstrong, R. C. and Hassager, O. 'Dynamics of Polymeric Liquids: Kinetic Theory', 2nd Edn, Vol. 2, Wiley, New York, 1987
2 Dotson, P. *J. Chem. Phys.* 1983, **79**, 5730
3 Saab, H. H. and Dotson, P. J. *J. Chem. Phys.* 1987, **86**, 3039
4 Liu, T. W. *J. Chem. Phys.* 1989, **90**, 5826
5 Zylca, W. and Öttinger, H. C. *J. Chem. Phys.* 1989, **90**, 474

6 Zylca, W. *J. Chem. Phys.* 1991, **94**, 4628
7 Reese, H. R. and Zimm, B. H. *J. Chem. Phys.* 1990, **92**, 2650
8 Rudisill, J. W. and Cummings, P. T. *J. Non-Newtonian Fluid Mech.* 1992, **41**, 275
9 Díaz, F. G., García de la Torre, J. and Freire, J. J. *Polymer* 1989, **30**, 259
10 López Cascales, J. J. and García de la Torre, J. *Macromolecules* 1990, **23**, 809
11 López Cascales, J. J. and García de la Torre, J. *Polymer* 1991, **32**, 3359
12 López Cascales, J. J., Navarro, S. and García de la Torre, J. *Macromolecules* 1992, **25**, 3574
13 López Cascales, J. J. PhD Thesis, University of Murcia, Spain, 1991
14 López Cascales, J. J. and García de la Torre, J. *J. Chem. Phys.* 1991, **95**, 9384
15 López Cascales, J. J. and García de la Torre, J. *J. Chem. Phys.* 1992, **97**, 4549
16 Fraenkel, G. K. *J. Chem. Phys.* 1952, **20**, 642
17 Warner Jr, H. R. *Ind. Eng. Chem., Fundam.* 1972, **11**, 379
18 Wedgewood, L. E., Ostrov, D. N. and Bird, R. B. *J. Non-Newtonian Fluid Mech.* 1991, **40**, 119
19 Ermak, D. L. and McCammon, J. A. *J. Chem. Phys.* 1978, **69**, 1352
20 Iniesta, A. and García de la Torre, J. *J. Chem. Phys.* 1990, **92**, 2015
21 Rotne, J. and Prager, S. *J. Chem. Phys.* 1969, **50**, 4831
22 Yamakawa, H. *J. Chem. Phys.* 1970, **53**, 436
23 Wang, S. J. *J. Chem. Phys.* 1990, **92**, 7618
24 Lindner, P. and Oberthür, R. C. *Colloid Polym. Sci.* 1988, **266**, 886
25 Kramers, H. A. *Physica* 1944, **11**, 1
26 Zylca, W. and Öttinger, H. C. *Macromolecules* 1991, **24**, 484
27 Farrell, C. J., Keller, A., Miles, M. J. and Pope, D. P. *Polymer* 1980, **21**, 129
28 Keller, A. and Odell, A. *Colloid Polym. Sci.* 1985, **263**, 181
29 Wiest, J. M., Wedgewood, L. E. and Bird, R. B. *J. Chem. Phys.* 1989, **90**, 1